Basic Res Cardiol (2013) 108:309
DOI 10.1007/s00395-012-0309-x

ORIGINAL CONTRIBUTION

# Selective inhibition of Cx43 hemichannels by Gap19 and its impact on myocardial ischemia/reperfusion injury

**Nan Wang · Elke De Vuyst · Raf Ponsaerts · Kerstin Boengler · Nicolás Palacios-Prado · Joris Wauman · Charles P. Lai · Marijke De Bock · Elke Decrock · Mélissa Bol · Mathieu Vinken · Vera Rogiers · Jan Tavernier · W. Howard Evans · Christian C. Naus · Feliksas F. Bukauskas · Karin R. Sipido · Gerd Heusch · Rainer Schulz · Geert Bultynck · Luc Leybaert**

Received: 9 July 2012 / Revised: 12 October 2012 / Accepted: 22 October 2012 / Published online: 8 November 2012


**Abstract** Connexin-43 (Cx43), a predominant cardiac connexin, forms gap junctions (GJs) that facilitate electrical cell–cell coupling and unapposed/nonjunctional hemichannels that provide a pathway for the exchange of ions and metabolites between cytoplasm and extracellular milieu. Uncontrolled opening of hemichannels in the plasma membrane may be deleterious for the myocardium and blocking hemichannels may confer cardioprotection by preventing ionic imbalance, cell swelling and loss of critical metabolites. Currently, all known hemichannel inhibitors also block GJ channels, thereby disturbing electrical cell–cell communication. Here we aimed to characterize a nonapeptide, called Gap19, derived from the cytoplasmic loop (CL) of Cx43 as a hemichannel blocker and examined its effect on hemichannel currents in cardiomyocytes and its influence in cardiac outcome after ischemia/reperfusion. We report that Gap 19 inhibits Cx43 hemichannels without blocking GJ channels or Cx40/pannexin-1 hemichannels. Hemichannel inhibition is due to the binding of Gap19 to the C-terminus (CT) thereby preventing intramolecular CT–CL interactions. The peptide inhibited Cx43 hemichannel unitary currents in both HeLa cells exogenously expressing Cx43 and acutely isolated pig ventricular cardiomyocytes. Treatment with Gap19 prevented metabolic

N. Wang, E. De Vuyst, R. Ponsaerts contributed equally.
G. Bultynck, L. Leybaert share senior authorship.

T. Miura, Sapporo, Japan served as guest editor for the manuscript and was responsible for all editorial decisions, including the selection of reviewers. The policy applies to all manuscripts with authors from the editor's institution.

**Electronic supplementary material** The online version of this article (doi:10.1007/s00395-012-0309-x) contains supplementary material, which is available to authorized users.

N. Wang · E. De Vuyst · M. De Bock · E. Decrock · M. Bol · L. Leybaert (✉)
Faculty of Medicine and Health Sciences, Physiology group, Department of Basic Medical Sciences, Ghent University, De Pintelaan 185 (Block B-Rm 310), B-9000 Ghent, Belgium
e-mail: Luc.Leybaert@UGent.be

R. Ponsaerts · G. Bultynck
Laboratory of Molecular and Cellular Signaling, Department of Cellular and Molecular Medicine, Campus Gasthuisberg, Katholieke Universiteit Leuven, O/N-1 bus 802, KU Leuven, Leuven, Belgium

K. Boengler · R. Schulz
Physiologisches Institut, Justus-Liebig Universität Giessen, Giessen, Germany

N. Palacios-Prado · F. F. Bukauskas
Dominick P. Purpura Department of Neuroscience, Albert Einstein College of Medicine, Bronx, NY, USA

J. Wauman · J. Tavernier
Faculty of Medicine and Health Sciences, Cytokine Receptor Laboratory, VIB Department of Medical Protein Research, Ghent University, Ghent, Belgium

C. P. Lai
Neuroscience Program, Departments of Neurology and Radiology, Massachusetts General Hospital, Harvard Medical School, Charlestown, MA, USA

M. Vinken · V. Rogiers
Faculty of Medicine and Pharmacy, Department of Toxicology, Vrije Universiteit Brussel, Brussels, Belgium

W. H. Evans
Department of Medical Biochemistry and Immunology, Cardiff University School of Medicine, Cardiff, UK

inhibition-enhanced hemichannel openings, protected cardiomyocytes against volume overload and cell death following ischemia/reperfusion in vitro and modestly decreased the infarct size after myocardial ischemia/reperfusion in mice in vivo. We conclude that preventing Cx43 hemichannel opening with Gap19 confers limited protective effects against myocardial ischemia/reperfusion injury.

**Keywords** Connexin · Hemichannel · Gap junction · Single channel · Myocardial injury

## Introduction

Gap junction (GJ) channels are essential for the function of the heart and blood vessels by providing electrical coupling and direct cell–cell transfer of chemical/metabolic signals [20, 32, 45, 74]. They are composed of two docked hemichannels (connexons) oligomerized from six connexin molecules. The 43-kDa connexin protein (Cx43) is a major connexin in the heart and is especially abundant in ventricular cardiomyocytes [15]. Aging and cardiac disease are associated with alterations in Cx43 expression, its localization and its phosphorylation status, and changes of GJ properties that, collectively, are thought to contribute to myocardial infarction injury and arrhythmogenesis [35, 64, 71]. Beyond GJs, emerging evidence has suggested novel roles of Cx43 hemichannels in the diseased myocardium. These unapposed/nonjunctional hemichannels reside in the zone surrounding the GJ nexus area called the perinexus [55]. They are typically closed under normal conditions, but may open in response to ischemic insults resulting in ATP leakage, excessive entry of $Na^+$ and $Ca^{2+}$ and the loss of essential metabolites from the cells [58]. Uncontrolled activation of hemichannels may potentially introduce significant changes in cardiamyocyte homeostasis that are expected to cause dysfunction and finally irreversible injury. Currently, there are no tools available that allow selective targeting of hemichannels, as all known pharmacological blockers inhibit both GJs and hemichannels [26, 27, 68]. Furthermore, connexin knockout (KO) technology abolishes hemichannels, as well as GJ channels making this approach inappropriate to determine the role of hemichannels in cardiovascular disease.

Connexins are tetraspan membrane proteins that have two extracellular loops and one intracellular loop (CL). Synthetic peptides like Gap26 and Gap27 that mimic a short stretch of amino acids (AAs) on the extracellular loops have been introduced more than 15 years ago to inhibit GJs [78]. These peptides are thought to interact with yet undefined sequence on the extracellular loops of the connexin protein thereby preventing the docking of two hemichannels [24]. Gap26 and Gap27 peptides also inhibit unapposed hemichannels [77]; because the extracellular loops of unapposed hemichannels are unoccupied and freely available for interactions with these peptides, hemichannel inhibition often occurs before inhibition of GJs. Here we report on a peptide, called Gap19 that is identical to a short sequence present on the intracellular (cytoplasmic) loop of Cx43. Peptides mimicking cytoplasmic loop (CL) sequences have been used in the past as control peptides that do not inhibit GJs [47]. In agreement, we found that Gap19 did not reduce GJ coupling as measured with dual whole-cell voltage-clamp and dye transfer assays. Surprisingly, Gap19 strongly inhibited plasma membrane Cx43 hemichannels as exemplified by ATP release/dye uptake studies and unitary hemichannel current measurements. Surface plasmon resonance (SPR) experiments demonstrated that Gap19 interacts with the Cx43 C-terminus (CT) and hemichannel inhibition was counteracted by a peptide identical to the last 10 AAs of the CT, indicating that Gap19 inhibition of hemichannels is caused by preventing intramolecular interactions of the CT with the CL, which are essential for Cx43 hemichannel activities [49, 50]. Moreover, Gap19 inhibited the potentiation of unitary hemichannel currents in acutely isolated ventricular cardiomyocytes exposed to metabolic inhibition. In line with this finding, the peptide protected against myocardial cell swelling and cell death in in vitro cardiac ischemia/reperfusion studies and modestly limited the infarct size in in vivo cardiac ischemia/reperfusion in mice. Importantly, Gap19 had no effect on pannexin-1 (Panx1) or Cx40 hemichannels. Thus, Gap19 emerges as a novel tool to specifically block Cx43 hemichannels without inhibiting GJs, allowing in vitro and in vivo work aimed at determining the role of hemichannels in cardiac disease models, as well as in other tissues and organs that display a prominent Cx43 expression.

## Methods

An expanded Methods section is provided in the Online Resource.

C. C. Naus
Faculty of Medicine, Department of Cellular and Physiological Sciences, Life Sciences Institute, University of British Columbia, Vancouver, BC, Canada

K. R. Sipido
Division of Experimental Cardiology, Department of Cardiovascular Diseases, Katholieke Universiteit Leuven, Leuven, Belgium

G. Heusch
Institute for Pathophysiology, Universitätsklinikum Essen, Essen, Germany

### GJ coupling studies

GJ coupling was investigated by dye coupling and electrophysiological studies. Dye coupling was assessed by fluorescence recovery after bleaching (FRAP) and scrape loading of dye transfer (SLDT) [21]. For FRAP, confluent cell cultures were loaded with 5-carboxyfluorescein diacetate acetoxymethylester (CFDA-AM, 20 μM). Fluorescence within a single cell was photobleached by spot exposure to 488 nm Argon laser light. The fluorescent intensity in the bleached cell was followed over a 5-min period and quantified at the end of this period as the percentage of recovery relative to the starting level before bleaching. SLDT was performed by making a linear scratch across a confluent monolayer of cells in the presence of 6-carboxy fluorescein (6-CF, 0.4 mM). A fluorescence diffusion profile perpendicular to the scratch was recorded and the spatial constant of mono-exponential fluorescence decrease was determined as a measure of GJ coupling. The junctional electrical conductance between cells was measured as described in Ref. [8].

### Hemichannel studies

Hemichannel opening was investigated by ATP release studies and electrophysiological measurements of unitary hemichannel activity. ATP release was detected using a luciferin/luciferase assay kit (product no. FL-AA; Sigma-Aldrich, Bornem, Belgium) as previously described [17]. Hemichannel unitary currents were measured as described in Ref. [8]. For measurements in cardiomyocytes, KCl in the pipette solution was replaced by CsCl [38].

### Preparation of cardiomyocytes

Cardiomyocytes for patch-clamp experiments were isolated from left ventricles of domestic pigs (14–17 weeks) by enzymatic digestion [69]. The mouse cardiomyocytes used for in vitro ischemia/reperfusion studies were isolated by excising C57/BL6 mice (<3 months) hearts followed by cardiomyocyte isolation as described in Ref. [40].

### In vitro cardiomyocyte ischemia/reperfusion

Primary cardiomyocytes were isolated from mice as described in Ref. [40]. Cells were dispersed in isolation solution (0.025 mM $Ca^{2+}$) by gentle agitation. $Ca^{2+}$ in the solution was then gradually increased in small steps to 1 mM. Cardiomyocytes, sedimented to the bottom of a 10-ml tube, were exposed during 120 min to hypoxic ($N_2$-gassed), glucose-deprived acidic (pH 6.5) solution [oxygen-glucose deprivation (OGD)/acidosis solution] on top of which a layer of mineral oil was added. Reperfusion consisted of removing the mineral oil and replacing the OGD/acidosis solution by a normoxic solution (pH 7.4) for 3 min. After normoxia or OGD/acidosis, a 10-μl cell sample was taken and resuspended for 5 min in control solution with 0.5 % trypan blue. Images of cell morphology were obtained at 100× magnification on a Leica DMLB microscope (Leica, Bensheim, Germany). Cell viability was quantified as the percentage of rod-shaped, unstained cells over the total cell population by an examiner blinded to the different conditions. A total of at least 1000 cells were counted per group.

For volume measurements, the cardiomyocytes were loaded with 2 μM calcein-AM in normoxic solution (15 min, 35 °C) and were then scanned with a confocal microscope (Zeiss axiovert 100 M, Jena, Germany) at 40× magnification and Z-stacks were taken every 2 μm in 15 cells per group. The cell volume was expressed relative to the cell volume under normoxic conditions. Exposure to OGD/acidosis was 60 min and the normoxia/reperfusion condition was applied 15 min in these experiments.

### In vivo mouse model

The experiments were approved by the regional ethical committee. C57/BL6 mice were subject to 30 min ischemia and 120 min reperfusion [4]. The area at risk was determined by Evans Blue and the ischemic zone was visualized by 2,3,5-triphenyl tetrazolium chloride staining. Gap19 (MW 1161.44 Da) was intravenously administered at a concentration of 25 mg/kg, which corresponds to ~250 μM, assuming distribution in the blood volume that is approximately 8 % of the body weight (blood volume values were in the 1.6–2 ml range). The 250-μM concentration gives an expected 97 % inhibition based on the data presented in Fig. 1d.

### Data analysis and statistics

The data are expressed as mean ± SEM, with '*n*' denoting the number of independent experiments. In the in vitro and in vivo ischemia experiments, '*n*' corresponds to the number of animals. Comparisons between two groups were done with a two-tailed unpaired *t* test; comparison of more than two groups was done with one-way ANOVA and a Bonferroni post hoc test; in the in vivo ischemia experiments a Fisher's Least Significant Difference test was used. A $p$ value <0.05 was considered as indicating statistical significance. In the graphs, statistical significance is indicated with a single symbol (* or #) for $p < 0.05$, two symbols for $p < 0.01$ and three symbols in case of $p < 0.001$.

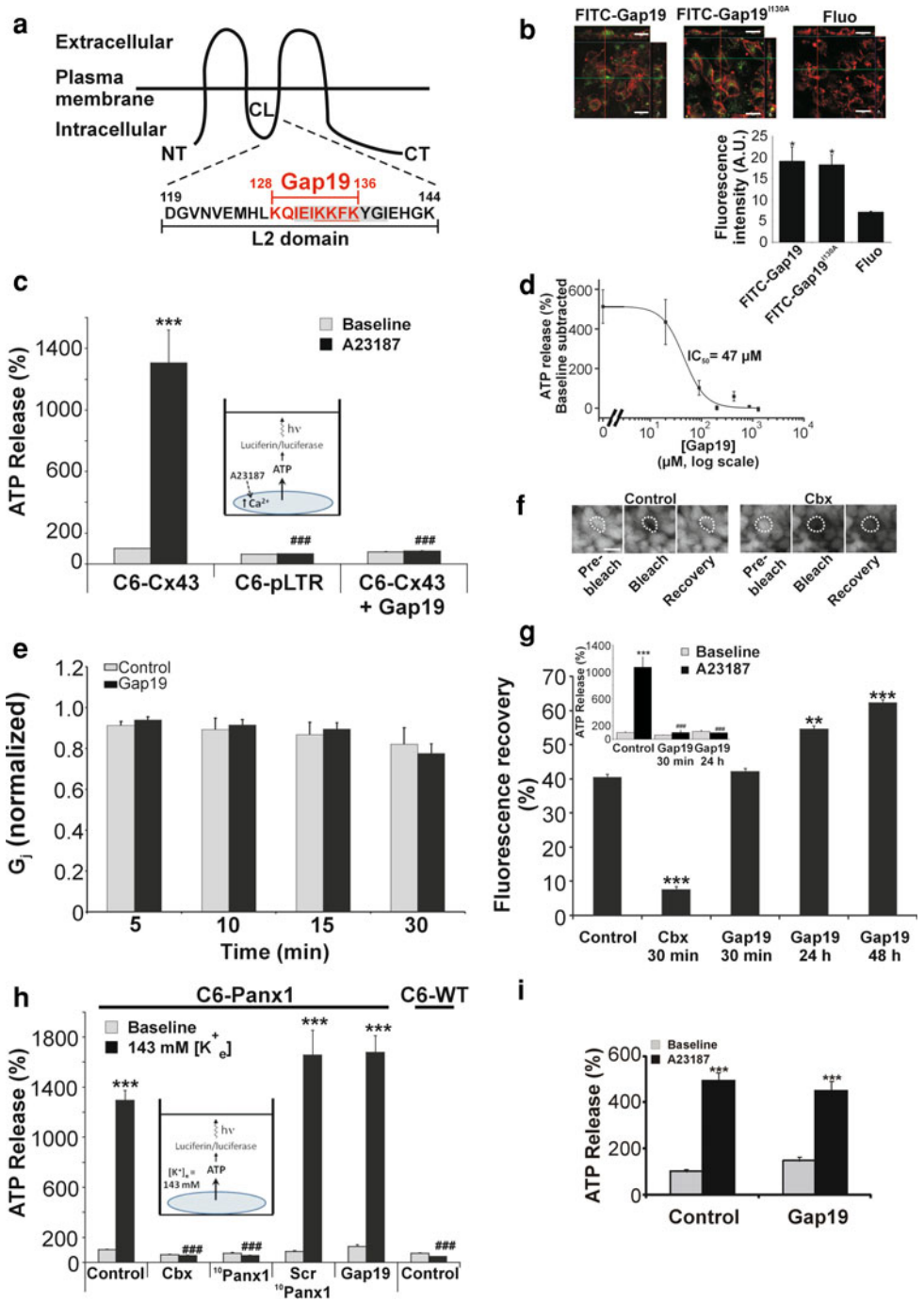


## Results

### Gap19 inhibits Cx43 hemichannel activity but not GJ coupling

Gap19 is a synthetic nonapeptide corresponding to AAs 128–136 in the second half of the CL of Cx43 and is part of the so-called L2 region [63] (Fig. 1a and Online Resource Table S1). Furthermore, AAs 130–136 are part of a sequence (AAs 130–139) that is important for CL interactions with the CT tail of Cx43 [7, 22, 31]. Gap19 contains the KKFK sequence that is a known cell-membrane translocation motif that facilitates plasma membrane permeability [9]. This may explain the higher uptake of Gap19 tagged with fluorescein isothiocyanate (FITC) in C6 glioma cells stably transfected with Cx43 (C6-Cx43) compared to fluorescein alone (Fig. 1b). We determined the effect of Gap19 on ATP release triggered by an elevation of the cytoplasmic $Ca^{2+}$ concentration ($[Ca^{2+}]_i$) caused by exposing C6-Cx43 cells (plated at low density)

◀ **Fig. 1** Gap19 inhibits $[Ca^{2+}]_i$-triggered ATP release in C6-Cx43 cells. **a** Topology of Cx43 and location of Gap19 in the L2 domain, part of the CL. The *underlined* sequence is a putative membrane translocation motif and the *greyed zone* is crucial for CT–CL interactions. **b** Confocal micrographs of C6-Cx43 cells, counter-stained for F-actin (*red fluorescence*), illustrating cellular uptake of fluorescein-labeled (*green*) Gap19 (FITC-Gap19), Gap19I$^{130A}$ (FITC-Gap19$^{130A}$) and fluorescein only (Fluo). *Scale bar* is 20 μm. The *bar chart* below reports fluorescence intensities (A.U., arbitrary units) measured in the cells. Uptake of fluorescein-labeled peptides was significantly stronger as compared to fluorescein only ($n = 4$). *Stars* indicate significance compared to Fluo. **c** Inducing $[Ca^{2+}]_i$ changes with the $Ca^{2+}$ ionophore A23187 (*inset* shows experimental approach) triggered significant ATP release in C6-Cx43 but not in C6 cells stably transfected with the empty vector (C6-pLTR) ($n = 12$). Gap19 (200 μM, 30 min) strongly inhibited $[Ca^{2+}]_i$-triggered ATP release. **d** Gap19-inhibition of triggered ATP release was concentration-dependent ($n = 6$). **e** Junctional conductance ($G_j$) measurements in Cx43 expressing Novikoff cell pairs at different time points in the absence or presence of Gap19 (400 μM) in the recording pipette solution. $G_j$ was normalized to the corresponding values at the beginning of the experiment. Gap19 had no effect on $G_j$ ($n = 4$–16). **f** Representative images of a FRAP experiment in C6-Cx43 cells preloaded with CFDA. Images were acquired before photobleaching (pre-bleach), just after photobleaching the cell marked with the *dotted line* (bleach) and 5 min later to assess fluorescence recovery in the bleached cell. **g** Quantification of the fluorescence recovery 5 min after photobleaching: 30 min Gap19 (200 μM) had no influence while 24–48 h incubations promoted dye transfer ($n = 5$). *Inset* above illustrates that 24 h incubation with Gap19 inhibited ATP release equally strong as 30 min incubation ($n = 12$). **h** Exposure of C6-Panx1 cells to 143 mM $[K^+]_e$-triggered ATP release that was blocked by carbenoxolone (Cbx, 10 μM, 30 min) or $^{10}$Panx1 (200 μM, 30 min), and absent in C6-WT cells. Gap19 or Scr$^{10}$Panx1 had no effect on high $[K^+]_e$-triggered ATP release ($n = 12$). **i** Gap19 (200 μM, 30 min) did not inhibit $[Ca^{2+}]_i$-triggered ATP release (brought about by 2 μM A23187 applied during 5 min) in HeLa-Cx40 cells ($n = 6$). *Stars* indicate statistical significance compared to the neighboring *grey baseline bar* (except in **b**); *number signs* mark comparisons to the *black control bar*; one symbol $p < 0.05$, two symbols $p < 0.01$, three symbols $p < 0.001$

to the $Ca^{2+}$ ionophore A23187 (2.2 μM, 5 min, Fig. 1c, left bars), which, as reported, results in transient elevation of $[Ca^{2+}]_i$ to ~500 nM [19, 49]. $[Ca^{2+}]_i$-triggered ATP release in C6-Cx43 cells depends on Cx43 hemichannels because Cx43 knock-down [19] or transfection of C6 cells with the empty vector (pLTR) do not display these responses (Fig. 1c, middle bar). Online Resource Fig. S1A shows Cx43 expression in C6-pLTR and C6-Cx43 cells. Gap19 inhibited $[Ca^{2+}]_i$-triggered ATP release (Fig. 1c, right bars) in a concentration-dependent manner with a half-maximal effect ($IC_{50}$) of ~47 μM (Hill coefficient = 2) (Fig. 1d). Gap19 (400 μM applied via the pipette solution) did not inhibit the junctional conductance determined in Novikoff cell pairs (endogenously expressing Cx43) making use of dual-cell voltage-clamp (Fig. 1e). Cell-to-cell dye transfer studies with FRAP in C6-Cx43 cells confirmed that 30 min exposure to Gap19 (200 μM) had no effect on dye coupling (Fig. 1f, g). We verified higher Gap19 concentrations in FRAP experiments and found that 1 h exposure to concentrations of 10 μM to 1 mM Gap19 had no effect on dye coupling (Online Resource Fig. S1B). In fact, 24–48 h exposure to 200 μM Gap19 was found to promote dye coupling in FRAP studies (Fig. 1g). ATP release was still completely blocked following 24 h incubation with 200 μM Gap19 (inset to Fig. 1g). Gap19 did not inhibit ATP release triggered by exposure of C6 cells stably transfected with pannexin-1 (C6-Panx1) to high extracellular potassium concentration ($[K^+]_e = 143$ mM) (Fig. 1h). High $[K^+]_e$ is a known stimulus for Panx1 hemichannel opening [67] and control experiments confirmed that the triggered ATP release was suppressed by low concentrations of carbenoxolone (10 μM, 30 min) and $^{10}$Panx1 peptide (200 μM, 30 min), two blockers of Panx1 hemichannels [42, 48], but not by scrambled $^{10}$Panx1 (Scr$^{10}$Panx1) [70, 76] (Fig. 1h). Exposure of C6 wild type (WT) cells to high $[K^+]_e$ did not trigger ATP release above baseline (Fig. 1h—Online Resource Fig. S1A illustrates Panx1 expression in the cells used). Furthermore, Gap19 did not influence $[Ca^{2+}]_i$-triggered ATP release in HeLa cells expressing Cx40 (Fig. 1i), a major Cx expressed in the atrium and cardiac conducting system [64].

## Amino acids I130 and K134 are important for Gap19 activity

Gap19 contains two AAs known to be mutated in certain types of oculodentodigital dysplasia (ODDD), a Cx43-linked genetic disease [63, 65]. I130T mutation is linked to neurological abnormalities and associated with decreased GJ dye transfer and non-functional hemichannels [39, 65]. Moreover, I130 is involved in the formation of hydrogen bonds [22] indicating that this AA might be important for Gap19 activity. K134E mutation decreases the single-channel conductance of GJ channels and interferes with normal GJ plaque formation [63, 65]. We found that Gap19 containing the I130A modification (Gap19$^{I130A}$, concentrations as for Gap19) failed to inhibit $[Ca^{2+}]_i$-triggered ATP release (Fig. 2a). The cellular uptake of FITC-Gap19$^{I130A}$ was comparable to the uptake of FITC-Gap19 as illustrated in Fig. 1b. To determine the importance of neighboring AAs, we measured the effect of Gap19$^{E131A}$ and found it equally active as Gap19 (Fig. 2a). Since mutations of K134 may alter the membrane permeability of Gap19, we constructed a plasmid encoding Gap19 coupled via its N-terminus to a FLAG-tag (pFLAG-Gap19). In contrast to C6-Cx43 cells expressing pcDNA5/FRT-eGFP (empty vector), C6-Cx43 cells expressing pFLAG-Gap19 displayed no significant $[Ca^{2+}]_i$-triggered ATP release (Fig. 2b) and maintained normal GJ coupling measured with SLDT (Fig. 2c, d), similar to the results obtained with

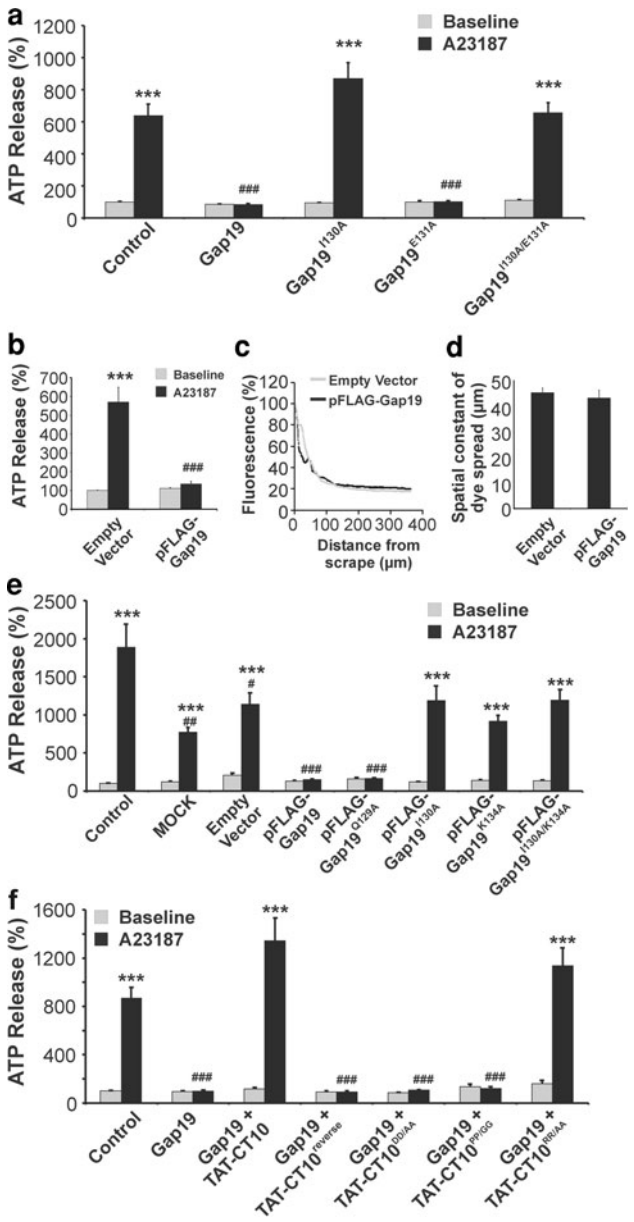


◀ **Fig. 2** Gap19 activity depends on AA 130 and 134 and is counteracted by adding CT10 peptide. **a** Gap19$^{I130A}$ (200 μM, 30 min) had no effect on $[Ca^{2+}]_i$-triggered ATP release in C6-Cx43 while Gap19$^{E131A}$ acted as Gap19. Combining the I130A/E131A modifications gave results as for Gap19$^{I130A}$ ($n = 12$). **b** Amino acid substitutions in the putative membrane translocation motif of Gap19 were tested using the pFLAG-Gap19 plasmid. $[Ca^{2+}]_i$-triggered ATP release was absent in C6-Cx43 cells transiently transfected with pFLAG-Gap19 ($n = 12$). **c** Example traces of SLDT dye (6-CF) spread experiments in C6-Cx43 cells (empty vector) and C6-Cx43 cells transfected with pFLAG-Gap19. **d** Quantification of the spatial constant of dye spread from SLDT experiments, demonstrating no effect of pFLAG-Gap19 on dye spread ($n = 3$; $p = 0.6337$). **e** pFLAG-Gap19$^{I130A}$ acted as Gap19$^{I130A}$ and did not inhibit $[Ca^{2+}]_i$-triggered ATP release while pFLAG-Gap19$^{Q129A}$ acted inhibitory. pFLAG-Gap19$^{K134A}$ did not inhibit $[Ca^{2+}]_i$-triggered ATP release; the combined I130A/K134A mutant acted as the single mutants ($n = 12$). **f** CT10 peptide counteracts Gap19 effects. In C6-Cx43 cells pre-incubated with TAT-CT10 (100 μM, 30 min), Gap19 (200 μM, 30 min together with TAT-CT10) did not inhibit ATP release while TAT-CT10$^{reverse}$ had no effect. The two aspartate and two proline residues in CT10 are crucial for this effect ($n = 12$). *Stars* compared to the neighboring *grey baseline bar*; *number signs* compared to the *black control bar* in **a** and **f**, and to the *black empty vector bar* in **b** and **e**

exogenously applied Gap19 peptide. In line with the results obtained with Gap19$^{I130A}$ (Fig. 2a), pFLAG-Gap19$^{I130A}$ failed to suppress ATP release (Fig. 2e). pFLAG-Gap19$^{Q129A}$ inhibited ATP release like pFLAG-Gap19, further supporting the notion that AAs neighboring I130 are not essential for hemichannel inhibition (Fig. 2e). Finally, pFLAG-Gap19$^{K134A}$ was ineffective as an inhibitor of ATP release (Fig. 2e). Thus, I130 and K134 are important AAs in the inhibitory effect of Gap19 on ATP release.

## Gap19 inhibition of hemichannels involves direct interactions with the CT tail

Since intramolecular interactions of the last ten AAs of the CT with the CL are important for Cx43 hemichannel function [49] and AAs 130–136 in the CL are involved in CT binding, we investigated whether Gap19 (AAs 128–136) blocks hemichannels by binding to the CT thereby preventing CT–CL interaction. Pre-incubating C6-Cx43 cells with membrane-permeable TAT-CT10 (100 μM, 30 min), a peptide corresponding to the last ten AAs of the Cx43 CT (Online Resource Table S1), followed by co-incubation with Gap19, completely abolished Gap19 inhibition of $[Ca^{2+}]_i$-triggered ATP release, while the peptide with reversed CT10 sequence (TAT-CT10$^{reverse}$) did not (Fig. 2f). Mutant versions of TAT-CT10 were designed to determine the residues critical for neutralizing Gap19 activity. The choice for particular mutants was based on the data of Hirst-Jensen et al. [31] pointing to the importance of residues in the 376–379 domain for CT–CL interactions. Modifying D378 and D379 to alanine residues (TAT-CT10$^{DD/AA}$) or P375 and P377 to glycine residues (TAT-CT10$^{PP/GG}$) resulted in peptides that failed to abolish Gap19 activity, while modifying R374 and R376 to alanine residues (TAT-CT10$^{RR/AA}$) had no effect (Fig. 2f). Similar results were obtained with pFLAG-Gap19 expression studies instead of exogenously applied Gap19 peptide (Online Resource Fig. S2). These results indicate that the two aspartate and two proline residues present in the last 10 AA-stretch of the CT are critical for Gap19-inhibitory actions.

It is known that the L2 region of the CL, in which sequence of Gap19 is located, is important for interactions with the CT [22, 31, 49]. We further explored Gap19-CT interactions with SPR and monitored the association of purified Cx43 CT tail (AAs 255–382) with biotin-Gap19 immobilized to a streptavidin-coated sensor chip. Immobilized biotin-L2

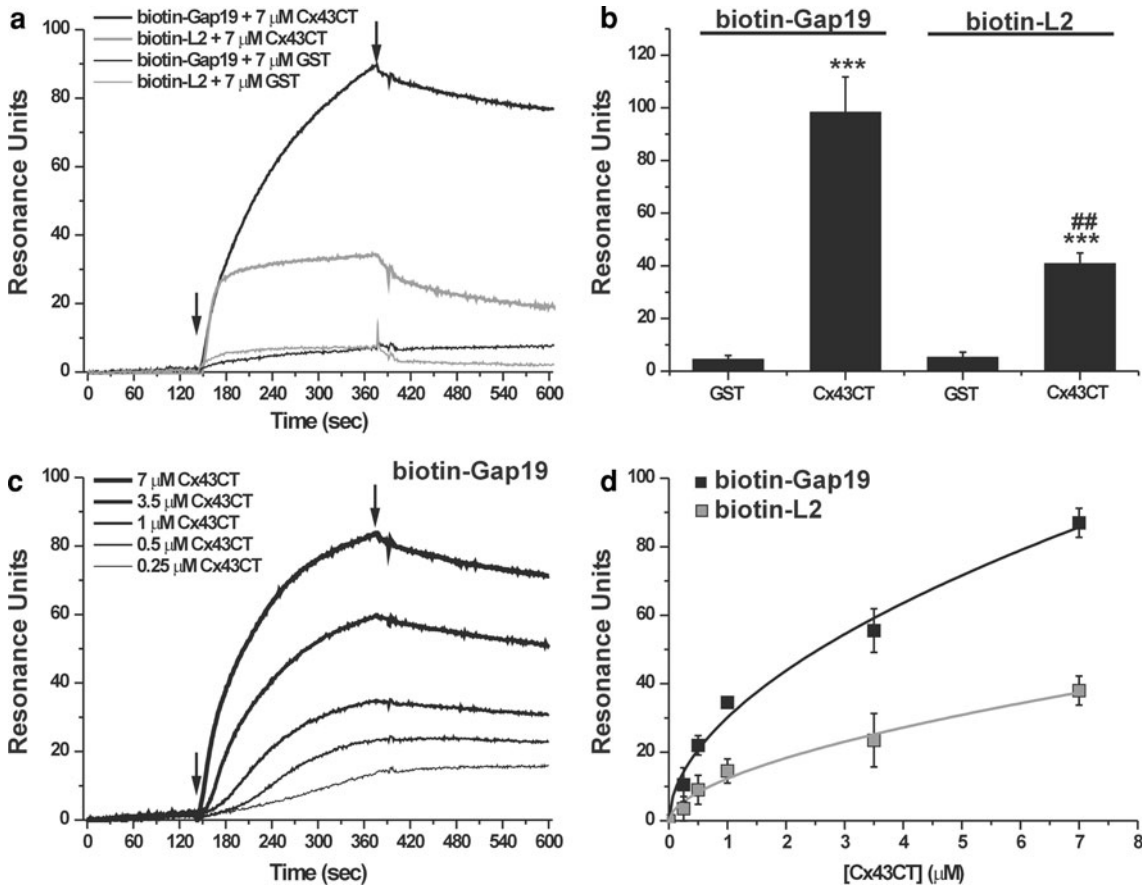


**Fig. 3** SPR experiments demonstrating Cx43 CT tail binding to biotin-Gap19 immobilized to a streptavidin-coated sensor chip. **a** Typical sensorgrams showing the association (*first arrow*) and dissociation (*second arrow*) between purified CT tail (Cx43CT, 7 μM) or purified GST (7 μM) and biotin-Gap19 or biotin-L2 immobilized to the streptavidin-coated sensor chip. The ordinate is calibrated in resonance units after correction for background binding to the control peptide (L2-reverse). **b** Summarized average data of experiments shown in **a** measured at maximal response (*second arrow*) ($n = 3$), demonstrating significantly stronger association between Cx43CT and Gap19 as compared to GST-Gap19. Cx43CT-Gap19 association was also stronger than for Cx43CT-L2. **c** Sensorgrams for Cx43CT-Gap19 and Cx43CT-L2 association at different concentrations of purified Cx43CT. **d** Summary of data shown in **c**, demonstrating a concentration-dependent increase in the association signal with half-maximal effect at ~2.5 μM for both Gap19 and L2 ($n = 3$)

(AAs 119–144) and its reversed sequence version were used as positive and negative controls, respectively. These experiments displayed a clear association of the CT tail with Gap19 and L2. Interestingly, the binding of the CT tail to Gap19 seemed stronger as compared to L2 (Fig. 3a, b). The CT-Gap19 association signal increased at higher concentrations of the CT tail indicating a bona fide specific interaction. From these results, an estimated $K_D$ of ~2.5 μM was obtained (Fig. 3c, d).

## Gap19 inhibits hemichannel unitary current activity in Cx43 expressing HeLa cells

We used HeLa cells stably transfected with Cx43 (HeLa-Cx43) to determine whether Gap19 inhibits unitary currents through hemichannels in voltage-clamp experiments [12], performed on solitary non-coupled cells, in the presence of extracellular $Ca^{2+}$ and $Mg^{2+}$, and under conditions of $K^+$-channel blockade (Fig. 4a). Application of voltage ramps showed that hemichannel currents appeared at potentials above +50 mV (Fig. 4b) and we chose +70 mV as a command voltage for subsequent experiments. Applying a depolarizing voltage step from −30 to +70 mV triggered unitary current events characterized by a conductance of ~220 pS (Fig. 4c, d), which corresponds to the single-channel conductance of Cx43 hemichannels [12]. The activity of unitary events was reduced when Gap19 (400 μM) was present in the pipette solution, while $Gap19^{I130A}$ had no effect (Fig. 4c). Unitary event activity often displayed multiple superimposed stepwise channel openings, which were less frequent with Gap19. Figure 4d (graphs in left column) illustrates that Gap19 decreased the number of peaks in the conductance histograms and increased the frequency of the closed state. Figure 4d (graphs

in right column) demonstrates that Gap19 did not influence the time constant of open dwell-time distributions while clearly decreasing the number of channel openings. Integration of the current versus time traces, which yields the membrane charge transfer ($Q_m$) associated with unitary current activity, showed that Gap19 significantly suppressed $Q_m$ to ~25 % of the control level, whereas $Gap19^{I130A}$ had no effect (Fig. 4e). Online Resource Fig. S3A illustrates that the effect of Gap19 was rapid within 1 min. Gap19 inhibited $Q_m$ in a concentration-dependent manner with an $IC_{50}$ of ~6.5 μM (Hill coefficient = 2) (Fig. 4f). By contrast, $Gap19^{I130A}$ had no effect unless applied at 1 mM concentration at which point the flat $Q_m$ curve displayed a sharp decrease, presumably as a result of steric block of the channel pore (Fig. 4g). A separate set of experiments was performed in cell-attached patch mode, to determine the effect of Gap19 on the open probability ($P_{open}$) of single hemichannels. The $P_{open}$ was 0.01 ± 0.0004 for control recordings ($V_m$ steps to +70 mV) and 0.0009 ± 0.0003 with Gap19 present in the bath (200 μM, 30 min pre-incubation) demonstrating a significant ~10-fold reduction by Gap19 ($p < 0.0001$, $n = 5$).

## Gap19 inhibits hemichannel unitary currents in ventricular cardiomyocytes

We sought to identify single-channel Cx43 hemichannel activity in ventricular cardiomyocytes acutely isolated from adult pig heart, under recording conditions as applied in the experiments on HeLa-Cx43 cells but with CsCl instead of KCl as the main pipette salt. Voltage steps from −70 mV to $V_m$ in the range of +10 to +100 mV triggered single-channel current activity from $V_m = +30$ mV on, with a single-channel conductance of ~200 pS as judged from conductance histograms (Fig. 5a). When Gap19 was added to the recording pipette (100 μM), unitary current activity was strongly decreased and voltage steps to more positive $V_m$ were necessary to observe unitary events (Fig. 5a). Figure 5b illustrates that, under control conditions without Gap19, stepping back from positive $V_m$ (applied 30 s) to −70 mV caused clearly discernible single-channel activity that was present during 100–200 ms; all-point histogram analysis indicated a ~200 pS unitary conductance (Fig. 5b). The recordings of single-channel activity at positive (during the $V_m$ step) and negative (tail currents) voltages allowed to construct a plot of unitary membrane current ($I_m$) as a function of $V_m$ (Fig. 5c). This open hemichannel $I_m$–$V_m$ plot demonstrated a linear relation characterized by a reversal potential of ~0 mV and a single-channel slope conductance of 196 ± 3.8 pS ($n = 7$) (Fig. 5c). We analyzed the voltage-dependence of unitary current activation under control and in the presence of Gap19 (100 μM) and found that the activation curve was shifted to the right by ~30 mV (Fig. 5d). Gap19 thus significantly increased the $V_m$ threshold for hemichannel activation. Although the unitary activity was strongly depressed by Gap19, sufficient data (at strong positive $V_m$ and in the tails at negative $V_m$) were available to construct an $I_m$–$V_m$ plot (Fig. 5e). This analysis revealed a reversal potential of ~0 mV and a single-channel slope conductance that was very similar to the ones obtained from control conditions (204 ± 10.4 pS; $n = 6$). Thus, Gap19 inhibits unitary currents by shifting the voltage-dependence of hemichannel opening without affecting the open channel properties. Hemichannel inhibition by Gap19 in cardiomyocytes was slower as compared to recordings obtained in HeLa-Cx43 and it took several minutes to attain maximal effect (Online Resource Fig. S3B). This is likely caused by the lower concentration of Gap19 (100 μM versus 400 μM for Hela Cx43), the larger cell size of cardiomyocytes and a possibly more restricted intracellular diffusion.

Metabolic inhibition (MI) with mitochondrial uncoupler carbonyl cyanide *p*-trifluoromethoxyphenylhydrazone (FCCP) combined with the glycolysis inhibitor sodium iodoacetate (IAA) ('chemical ischemia') activates hemichannel-related macroscopic currents and dye uptake in various cell types endogenously expressing Cx43 [13, 34, 38, 52]. We applied FCCP/IAA (5 μM and 1 mM respectively) and found it to strongly augment the unitary current activity recorded with $V_m$ steps to +40 mV (Fig. 5f). Most notably, when Gap19 was added in the pipette (100 μM), unitary activity was completely absent. Figure 5g summarizes average data from such experiments and shows that unitary current progressively increased upon prolonged exposure to MI while intracellular application of Gap19 abolished single-channel events throughout the recording.

## Gap19 protects against myocardial ischemia/reperfusion injury in vitro and in vivo

It has been reported that ischemic conditions trigger Cx43 hemichannel opening, possibly mediated by changes in the phosphorylation status of Cx43 and the generation of reactive oxygen and nitrogen species [28, 51, 54, 66]. We explored whether Gap19 could prevent possible deleterious effects of uncontrolled opening of hemichannels, thereby reducing ischemia/reperfusion damage to the myocardium in in vitro and in vivo studies. Exposing isolated cardiomyocytes to 120 min OGD and acidosis (pH 6.5) followed by a switch to control/normoxic solution (3 min) to simulate reperfusion resulted in extensive cell death (example image shown in Online Resource Fig. S4) with 10.9 % of the cardiomyocytes remaining viable (Fig. 6a). Cardiomyocytes exposed to normoxic solution over the same time period as OGD/acidosis showed no decline in survival (Fig. 6a). Pre-treatment of the cells with Gap19 (250 μM,

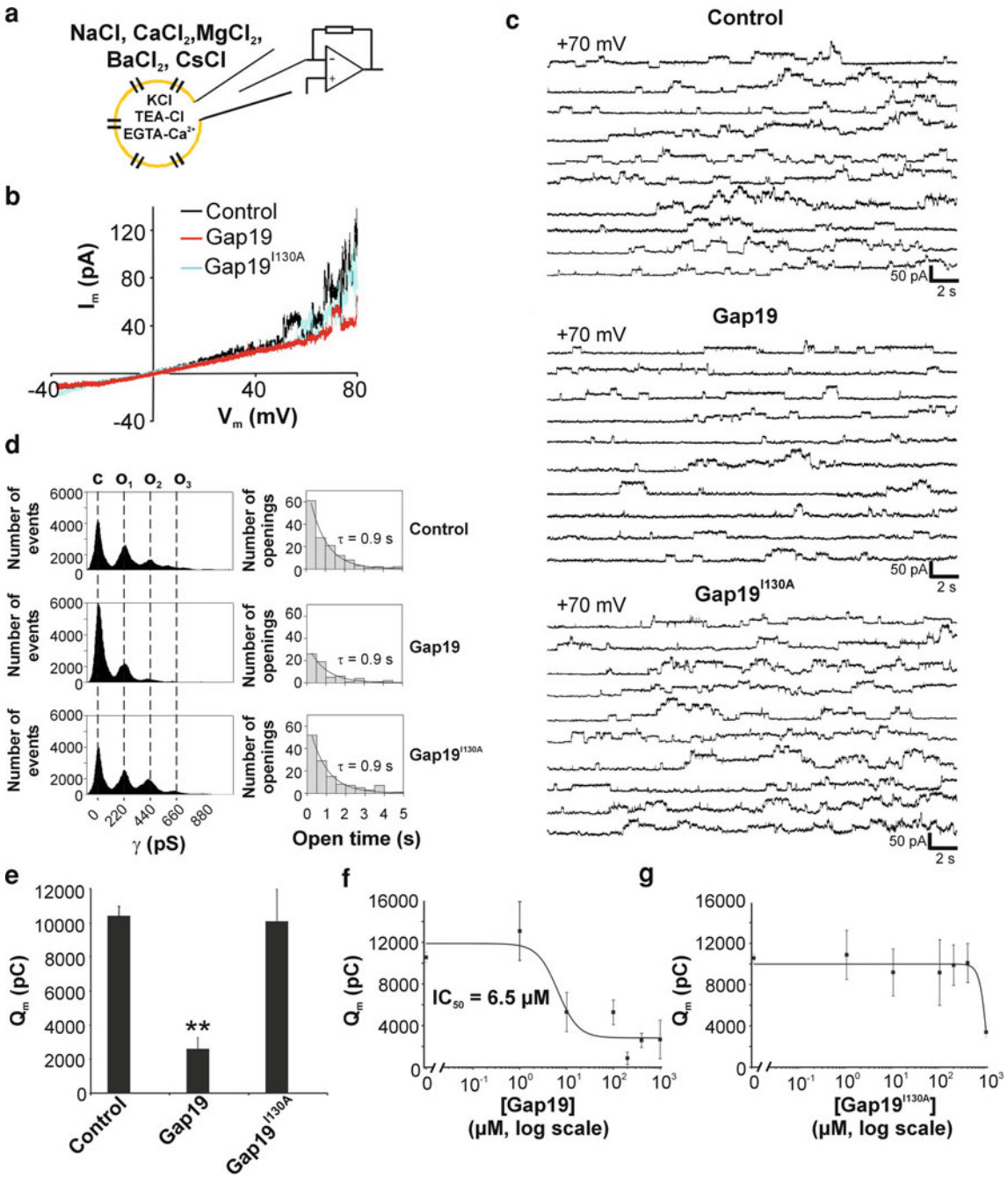


**Fig. 4** Gap19 inhibits unitary hemichannel currents in HeLa-Cx43 cells. **a** Whole-cell voltage-clamp recording conditions. **b** $I_m-V_m$ plot illustrating voltage ramp experiments (−40 to +80 mV, 70 s). Unitary current activity started to appear at +50 mV (control) and was enhanced by further increasing $V_m$. Experiments with Gap19 or Gap19$^{I130A}$ in the pipette solution (400 µM) are also shown. **c** Typical traces of unitary currents activated by stepping $V_m$ from −30 mV to +70 mV for 30 s. Ten consecutive runs (traces) were recorded over 7 min under control conditions (*top*) and when the pipette solution contained Gap19 (*middle*) or Gap19$^{I130A}$ (*bottom*). **d** *Left*: All-point histograms determined from each set of recordings depicted in **c**. *Dashed vertical lines* mark peaks in the histograms separated by ~220 pS. Gap19 reduced hemichannel activity as can be appreciated from the decreased number of peaks and increased frequency of the closed state. *Right*: Open dwell-time histograms determined from the recordings in **c**. Gap19 decreased the frequency of openings but had no effect on the time constant (τ) of the mono-exponential distribution of open dwell-times. Distributions with Gap19$^{I130A}$ were as observed in control. Data in **c** and **d** are representative for three different experiments. **e** *Bar chart* summarizing the results of integrating the current traces over time, giving the membrane charge transfer ($Q_m$), for the different conditions applied. Gap19 significantly suppressed $Q_m$ to ~1/4 of control while Gap19$^{I130A}$ had no effect ($n = 6$ for control, 8 for Gap19 and 6 for Gap19$^{I130A}$). **f** Gap19 inhibited $Q_m$ in a concentration-dependent manner. **g** $Q_m$ was not influenced by Gap19$^{I130A}$ unless it was applied at 1 mM concentration

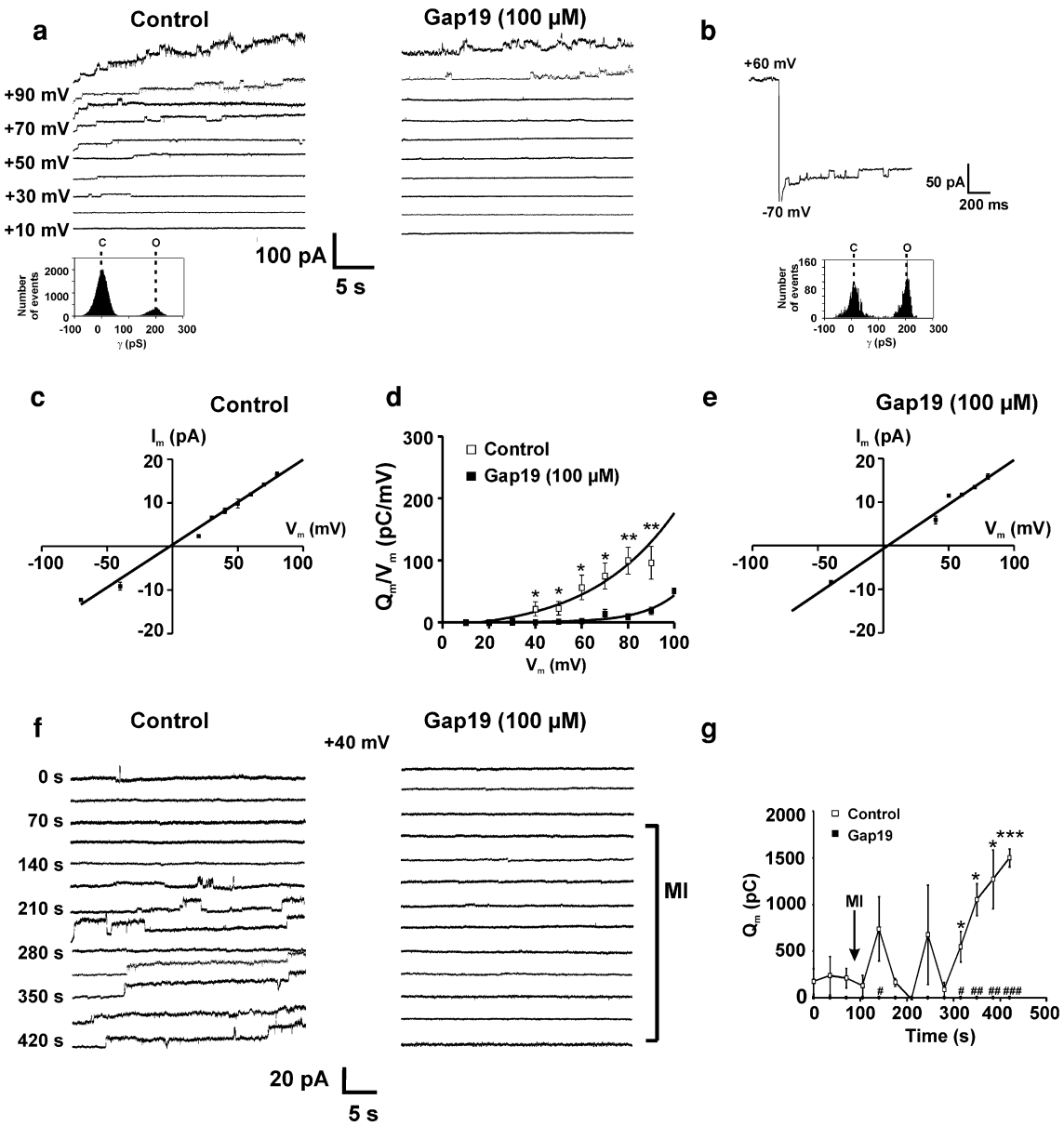


**Fig. 5** Gap19 inhibits hemichannel unitary currents in ventricular cardiomyocytes. **a** Whole-cell recording performed in acutely isolated ventricular cardiomyocytes revealed a $V_m$ dependent activation of Cx43 hemichannels (30 s voltage steps—traces representative for seven similar recordings). The all-point histogram illustration below the traces indicates a ~200 pS unitary conductance at $V_m = +30$ mV. In the presence of Gap19 (100 µM in the pipette), $V_m$ steps to more positive potentials were necessary (traces representative for six similar recordings). **b** Example traces illustrating that unitary current activities was still present after repolarizing to −70 mV. The all-point histogram below indicates a ~200 pS unitary conductance of the unitary tail current events. **c** $I_m - V_m$ plot of open hemichannels demonstrating a reversal potential of ~0 mV and a single-channel slope conductance of ~196 pS. **d** Voltage dependent activation of hemichannels, demonstrating that Gap19 (100 µM) shifted the activation curve to more positive potentials. The quantity $Q_m/V_m$ was calculated by dividing the integrated unitary current activity by the corresponding $V_m$, and represents the integrated single-channel conductance over the 30 s voltage steps ($n = 6$). **e** Gap19 inhibition of unitary events did not influence the open hemichannel $I_m - V_m$ plot (~0 mV reversal potential and 204 pS single-channel slope conductance, not different from control). **f** Example traces recorded in a cardiomyocyte before and after exposure to MI (5 µM FCCP and 1 mM IAA). Voltage steps from −70 mV (5 s) to +40 mV (30 s) were repetitively applied. Unitary current activity was completely absent with Gap19 in the recording pipette. **g** Summary *graph* illustrating progressively increasing unitary current activity after application of MI ($n = 4$). *Stars* indicate statistical significance compared to baseline before MI induction. Recordings with Gap19 in the pipette were flat, lacking any unitary activity, also after MI induction (*filled squares* on the abcis). Gap19 completely suppressed MI-promoted hemichannel activity. *Number signs* indicate statistical significance compared to the corresponding *open squares* recorded without Gap19 in the pipette

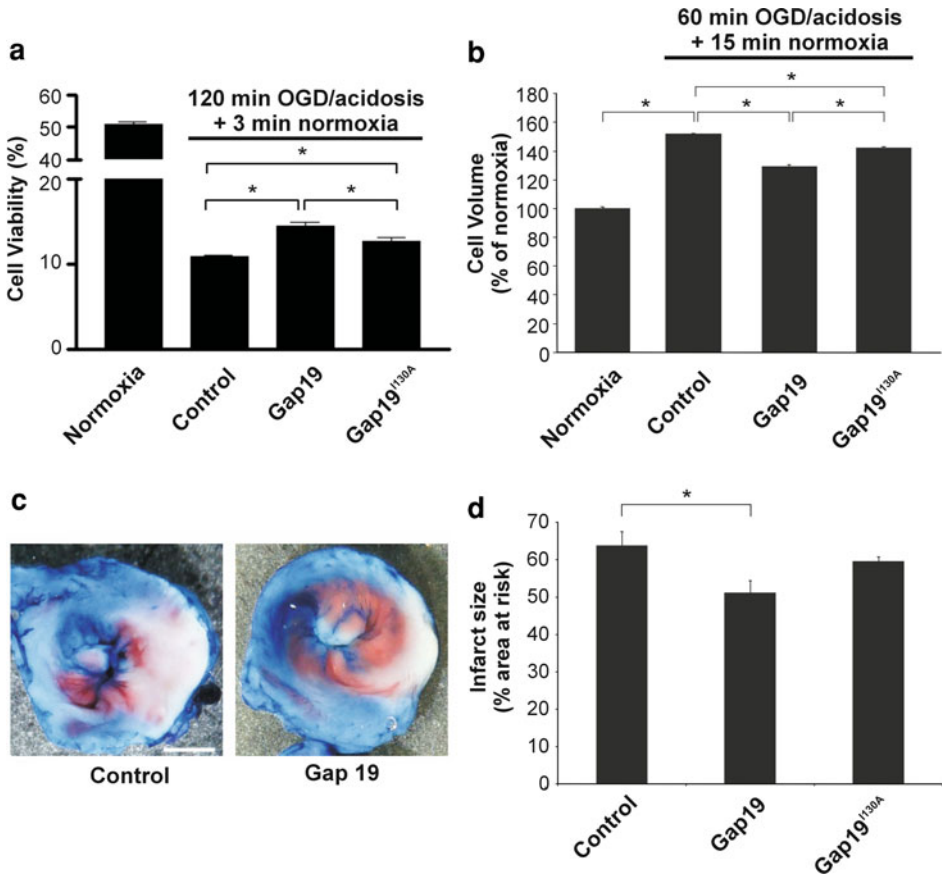


**Fig. 6** Gap19 improves cardiomyocyte viability following ischemia/reperfusion in vitro and in vivo. **a** In vitro simulated ischemia/reperfusion of isolated cardiomyocytes. Gap19 (250 μM, 30 min pre-incubation and present during OGD/acidosis) improved cardiomyocyte viability after 120 min OGD/acidosis (ischemia) followed by 3 min normoxia (reperfusion) compared to control cells treated with vehicle-only; $Gap19^{I130A}$ had less effect ($n = 6$). **b** OGD/acidosis + normoxia caused significant swelling of cardiomyocytes compared to normoxia. Pre-incubation of cardiomyocytes with Gap19 reduced the degree of cell swelling while $Gap19^{I130A}$ had less effect (250 μM, 30 min) ($n = 7$). **c** In vivo experiments in mice with LAD ligation for 30 min followed by 120 min reperfusion. Images of a representative experiment illustrating a reduction of the infarct area are marked *white* (TTC staining). *Red color* indicates viable tissue and *blue* represents perfused tissue. *Red* and *white zones* together form the area at risk. *Scale bar* is 1 mm. **d** Summary data of experiments illustrated in **c**. The infarct size, relative to the area at risk, was reduced by Gap19 injected intravenously (25 mg/kg) 10 min prior to the ligation, while $Gap19^{I130A}$ had no significant effect ($n = 11$ for control, 5 for Gap19 and 8 for $Gap19^{I130A}$)

30 min) followed by OGD/acidosis (with Gap19 present) and reperfusion (normoxia) increased the viability to 14.6 % thus enhancing the viability by approximately one-third as compared to treatment with vehicle-only (Fig. 6a). Exposing isolated cardiomyocytes to OGD/acidosis (60 min) followed by reperfusion (15 min) resulted in significant cell swelling that was counteracted by Gap19 (treatment as in the viability assays) (Fig. 6b). Gap19 did not affect the cell volume under normoxic conditions (99.1 ± 1.8 % compared to 100 ± 2.2 % in control, $n = 5$). $Gap19^{I130A}$ exhibited some protective effect against cell death and cell swelling but the effect of Gap19 was significantly stronger (Fig. 6a, b). We performed myocardial ischemia/reperfusion experiments in mice in vivo, by applying a 30 min ligation of the left anterior descending (LAD) coronary artery followed by reperfusion (120 min). Gap19 was intravenously injected 10 min before ligation at a dose of 25 mg/kg, corresponding to an estimated 250 μM concentration when distributed in the blood volume. This significantly reduced the infarct size to 51.2 %, compared to 63.8 % infarct size in vehicle-treated control animals, i.e. a reduction by approximately one-fifth. $Gap19^{I130A}$ had no significant effect compared to control (Fig. 6c).

## Discussion

Our data show that Gap19 blocks Cx43 hemichannels without inhibiting GJs, at micromolar concentrations ($IC_{50}$ of 6.5 μM) when applied intracellulary. This corresponds well to the ~2.5 μM $K_D$ value for interaction of Gap19

with its intracellular target which is the Cx43 CT tail. The $IC_{50}$ of extracellulary applied Gap19 is higher, presumably because of incomplete permeation through the plasma membrane. Online Resource Fig. S5 shows that the $IC_{50}$ of Gap19 linked to the TAT translocation motif, to further improve its membrane permeability, is $\sim$7 μM. Thus, micromolar intracellular Gap19 concentrations interact with the CT and inhibit hemichannels. Hemichannel inhibition is not caused by steric block of the channel pore by the peptide, because (1) the mutant peptide $Gap19^{I130A}$ had no effect unless applied at 1 mM concentration, (2) CT peptide (TAT-CT10) removed Gap19 inhibition, (3) the single hemichannel conductance was not altered by Gap19, and (4) Cx43-based GJs were unaffected. The effect of Gap19 was selective as it had no effect on hemichannels composed of Cx40 or Panx1. Cx40 is a major Cx in the atria, with a long CT as Cx43 and a slightly lower MW; Panx1 hemichannels have also been reported to be expressed in atrial cardiomyocytes [36]. The selectivity of Gap19 probably relates to the fact that the intracellular domains of the Cx protein are the least conserved region in contrast to the extracellular domains [1].

The molecular basis of the differential effect of Gap19 on hemichannels and GJs is related to the binding of this peptide to the CT tail which prevents CT–CL interaction. Disrupting CT–CL interaction results in reduced hemichannel openings and ATP release as demonstrated here, while avoiding closure of GJ channels as reported by others [63] and confirmed in the present experiments. The mechanisms underlying this differential regulation of hemichannels and GJs by CT–CL interactions are still unclear. However, it is important to notice that disrupting CT–CL interactions by CT-truncation of Cx43 has similar consequences: GJs remain functional [43], while hemichannels become resistant to activation [18, 49]. We anticipate that nonjunctional hemichannels (closed) may adopt different conformations as compared to those incorporated into GJs (open) [72, 73]. Interactions between subunits during docking of two hemichannels are indeed likely to result in conformational changes of the Cx protein and thereby alter gating [10, 23]. Another element that may contribute is the fact that hemichannels and GJ channels are differentially distributed over plasma membrane domains with slightly different properties, for example lipid rafts [3, 41]. Alternatively, Gap19 treatment may result in a reduction of the hemichannel population in the nonjunctional plasma membrane, e.g. due to accelerated incorporation into GJs or internalization. However, we found that the density of unapposed/nonjunctional hemichannels rather increased upon ectopic expression of pFLAG-Gap19 in C6-Cx43 cells (Online Resource Fig. S6). This figure also demonstrates increased phosphorylation of the hemichannel population with pFLAG-Gap19, which may well contribute to hemichannel inhibition[54] and may counteract decreased phosphorylation associated with ischemia [34, 38, 66].

Limited data are currently available demonstrating that nonjunctional membrane hemichannels in cardiomyocytes can open under certain conditions. The observation of a $[Ca^{2+}]_i$-dependent non-selective, macroscopic membrane current in rabbit ventricular myocytes in response to MI initially suggested Cx43 hemichannel opening in the heart [34, 38]. More recent findings report a marked increase of cell permeability based on ATP release and dye uptake associated with activated hemichannels in simulated ischemia of neonatal cardiomyocytes [11, 33, 66]. Here we demonstrate in ventricular cardiomyocytes single-channel plasma membrane currents with a unitary conductance of $\sim$200 pS in response to stepping $V_m$ to +30 mV and above. The biophysical properties of the observed unitary activity point to Cx43 hemichannels: (1) the single-channel conductance determined from histogram analysis or $I_m-V_m$ plot measurements was similar as observed in Hela cells overexpressing Cx43 and corresponds to approximately twice the single-channel conductance of Cx43 GJ channels; (2) currents reverse around 0 mV, indicating a non-selective ion channel; (3) unitary currents are inhibited by Gap19 as in HeLa-Cx43 cells. Interestingly, unitary hemichannel activity was also present in the tail currents during repolarization from positive voltage steps which may be caused by increased $[Ca^{2+}]_i$ that is known to potentiate hemichannel opening if <500 nM [19] or slow deactivation kinetics. Gap19 inhibited unitary hemichannel opening events and this was mainly related to an increased (more positive) voltage threshold for hemichannel opening and not the consequence of channel pore block (no change in the single-channel conductance). Thus, Gap19 appears to alter the voltage-sensitivity of Cx43 hemichannel gating as a consequence of disrupted CT–CL interactions.

Of note, Gap19 inhibition of ATP release was complete (Fig. 1d) while inhibition of unitary hemichannel currents was incomplete at high concentrations (Fig. 4f). This may point to a more pronounced inhibitory effect on the passage of large MW substances as compared to ions. Such differences in the potency of inhibition have been reported by others: phosphorylation of Cx43 hemichannels by PKC limits the passage of sucrose (MW 342 Da, MW of ATP is 507 Da) but not of the smaller ethyleneglycol (MW 62) [2]. An alternative explanation is that ATP release may behave in a non-linear manner (for example by $Ca^{2+}$-or ATP-induced ATP release) as suggested by previous studies demonstrating complete inhibition of ATP release with only a 50 % reduction in Cx43 expression [19].

The unitary hemichannel currents were strongly potentiated by imposing MI. Earlier observations in a variety of primary cells endogenously expressing Cx43 have suggested elevated hemichannel activities during chemical ischemia

[13, 52, 75]. These studies are, however, less conclusive as the evidence was based on hemichannel-permeable dye uptake studies (<1 KDa) or macroscopic current measurements. Here we provide detailed analysis at the highest resolution in intact ventricular cardiomyocytes, demonstrating activation of hemichannel unitary currents under MI. Interestingly, our data demonstrate stimulated unitary Cx43 hemichannel activity at +30 mV and above, which is in the range of the +30–40 mV attained during the plateau phase of the cardiac action potential. Several molecular mechanisms have been put forward to underlie increased hemichannel activity: (1) ATP depletion in metabolically inhibited cells affects the phosphatase/kinase balance, leading to Cx43 dephosphorylation which favors an open channel conformation [2, 37]; (2) S-nitrosylation may contribute to enhanced channel activities [52, 53] and (3) an increased fraction of hemichannels at the cell surface as observed for both Cx32 and Cx43 hemichannels within minutes after MI could also account for stimulated unitary current activities [53, 59]. Most notably, the unitary hemichannel currents activated by depolarization to +40 mV and promoted by MI were completely blocked by Gap19. This complete block is likely the result of a Gap19-induced increase in activation potential for hemichannel opening, which is shifted ~30 mV in the positive direction and therefore results in complete disappearance of current activity at +40 mV. Thus, ischemic conditions and depolarization activate hemichannels and this is inhibited by Gap19. The in vitro and in vivo cardiac ischemia/reperfusion experiments demonstrated that Gap19 significantly counteracted cell swelling, cell death and development of myocardial infarction. Taking together the facts that excessive opening of hemichannels may accelerate cell death [14, 58] and that Gap19 counteracts hemichannel opening in cardiomyocytes suggests that the improved outcome after ischemia/reperfusion is related to inhibition of Cx43 hemichannels present in the sarcolemma.

Not only Cx43 proteins embedded in the sarcolemma, but also those reported in mitochondria have been proposed to contribute to the cardioprotective effect of ischemic preconditioning [30, 62], a procedure of repeated exposure to sub-lethal ischemic conditions [46, 57, 61, 80]. Cx43 has been reported to be located in the inner mitochondrial membrane [5, 6, 44, 56], possibly in the hemichannel configuration, and appears to influence mitochondrial $K^+$ fluxes thereby providing cardioprotective effects [44]. It is important to realize that the putative protective role of mitochondrial Cx43 has only been demonstrated in the context of ischemic preconditioning [61]; currently, there is no evidence that this could play a role in a single episode of ischemia/reperfusion as applied in the present study.

Considering all evidence, the present data strongly point to the inhibition of plasma membrane hemichannel opening by Gap19 as the mechanism responsible for its protective effects against cardiac ischemia/reperfusion injury. The degree of protection, however, appears to be modest as opposed to recent evidence indicating a stronger effect of two extracellular loop mimetic peptides, Gap26 and Gap27 [28, 29]. Gap26/27 peptides target Cx43 channels but may also influence those composed of Cx37 and Cx40 [16, 25, 79]. The lesser degree of specificity toward different connexins is related to the fact that the extracellular loop sequence they mimic is highly conserved among different connexins. Thus, Gap26/27 peptides may have targets other than Cx43 hemichannels that confer additional protective potential. Most notably in this context is the fact that Gap19 does not inhibit GJs and thereby circumvents potential pro-arrhythmogenic effects of decreased GJ coupling during ischemia/reperfusion [32, 60]. Obviously, it would be interesting to further substantiate the effects of Gap19 on hemichannels in the in vivo situation; however, single-channel measurements under those conditions are extremely difficult to perform because the large degree of cardiomyocyte coupling via GJs precludes reliable space clamp conditions.

The distinctive effects of Gap19 on GJs and hemichannels are of fundamental importance: GJs and hemichannels are composed of the same Cx subunits and KO animal technology influences both channel types equally. Here we report Gap19 as a novel tool allowing selective studies on the role of Cx43 hemichannels in normal and diseased heart. In addition, blocking of hemichannels with Gap19 opens an avenue for therapeutic applications, limiting cellular injuries during ischemia/reperfusion while preserving electrical and metabolic cell–cell communication that are vital for the normal function of the myocardium.

**Acknowledgments** Special thanks to K. Leurs, K. Vermeulen and K. Welkenhuyzen for superb technical support. We express our gratitude to Dr. B. Himpens for support, to Dr. P. Zimmermann for the use of the Biacore 2000, to Dr. P. Sorgen for providing the pGEX6p2-Cx43CT plasmid, to Dr. G. Antoons for support with experiments on pig myocytes, and to Dr. D. Laird and Dr. S. Penuela for providing the anti-Panx1 antibody. We are very grateful to A. Gadicherla and Dr. B. Nilius for critically reading and commenting the manuscript. Research supported by the Fund for Scientific Research Flanders, Belgium (FWO, grant nos. G.0354.07, G.0140.08, 3G.0134.09 and G.0298.11 N to L.L. and G.0545.08 to G.B.), the Interuniversity Attraction Poles Program (Belgian Science Policy, project P6/31 and P7/10 to K.R.S and L.L., and P7 to J.T. and G.B.), the Concerted Actions program at KULeuven (grant no. GOA/09/012 to G.B.), the German Research Foundation (Schu 843/7-2 to R.S.), the BFH grant (grant no. PG/01/1298 to W.H.E), the Heart & Stroke Foundation of BC & Yukon and the Canadian Institutes of Health Research to C.C.N. and NIH grants (HL084464 and NS072238 to F.F.B.).

**Conflict of interest** None.

## References


1. Abascal F, Zardoya R (2012) Evolutionary analyses of gap junction protein families. Biochim Biophys Acta Epub ahead of print doi:10.1016/j.bbamem.2012.02.007
2. Bao X, Lee SC, Reuss L, Altenberg GA (2007) Change in permeant size selectivity by phosphorylation of connexin 43 gap-junctional hemichannels by PKC. Proc Natl Acad Sci USA 104:4919–4924. doi:10.1073/pnas.0603154104
3. Barth K, Gentsch M, Blasche R, Pfuller A, Parshyna I, Koslowski R, Barth G, Kasper M (2005) Distribution of caveolin-1 and connexin43 in normal and injured alveolar epithelial R3/1 cells. Histochem Cell Biol 123:239–247. doi:10.1007/s00418-004-0727-4
4. Boengler K, Buechert A, Heinen Y, Roeskes C, Hilfiker-Kleiner D, Heusch G, Schulz R (2008) Cardioprotection by ischemic postconditioning is lost in aged and STAT3-deficient mice. Circ Res 102:131–135. doi:10.1161/CIRCRESAHA.107.164699
5. Boengler K, Dodoni G, Rodriguez-Sinovas A, Cabestrero A, Ruiz-Meana M, Gres P, Konietzka I, Lopez-Iglesias C, Garcia-Dorado D, Di LF, Heusch G, Schulz R (2005) Connexin 43 in cardiomyocyte mitochondria and its increase by ischemic preconditioning. Cardiovasc Res 67:234–244. doi:10.1016/j.cardiores.2005.04.014
6. Boengler K, Stahlhofen S, van de Sand A, Gres P, Ruiz-Meana M, Garcia-Dorado D, Heusch G, Schulz R (2009) Presence of connexin 43 in subsarcolemmal, but not in interfibrillar cardiomyocyte mitochondria. Basic Res Cardiol 104:141–147. doi:10.1007/s00395-009-0007-5
7. Bouvier D, Spagnol G, Chenavas S, Kieken F, Vitrac H, Brownell S, Kellezi A, Forge V, Sorgen PL (2009) Characterization of the structure and intermolecular interactions between the connexin40 and connexin43 carboxyl-terminal and cytoplasmic loop domains. J Biol Chem 284:34257–34271. doi:10.1074/jbc.M109.039594
8. Bukauskas FF, Kreuzberg MM, Rackauskas M, Bukauskiene A, Bennett MV, Verselis VK, Willecke K (2006) Properties of mouse connexin 30.2 and human connexin 31.9 hemichannels: implications for atrioventricular conduction in the heart. Proc Natl Acad Sci USA 103:9726–9731. doi:10.1073/pnas.0603372103
9. Carrigan CN, Imperiali B (2005) The engineering of membrane-permeable peptides. Anal Biochem 341:290–298. doi:10.1016/j.ab.2005.03.026
10. Chen-Izu Y, Moreno AP, Spangler RA (2001) Opposing gates model for voltage gating of gap junction channels. Am J Physiol Cell Physiol 281:C1604–C1613
11. Clarke TC, Williams OJ, Martin PE, Evans WH (2009) ATP release by cardiac myocytes in a simulated ischaemia model: inhibition by a connexin mimetic and enhancement by an antiarrhythmic peptide. Eur J Pharmacol 605:9–14. doi:10.1016/j.ejphar.2008.12.005
12. Contreras JE, Saez JC, Bukauskas FF, Bennett MV (2003) Gating and regulation of connexin 43 (Cx43) hemichannels. Proc Natl Acad Sci USA 100:11388–11393. doi:10.1073/pnas.1434298100
13. Contreras JE, Sanchez HA, Eugenin EA, Speidel D, Theis M, Willecke K, Bukauskas FF, Bennett MV, Saez JC (2002) Metabolic inhibition induces opening of unapposed connexin 43 gap junction hemichannels and reduces gap junctional communication in cortical astrocytes in culture. Proc Natl Acad Sci USA 99:495–500. doi:10.1073/pnas.012589799
14. Contreras JE, Sanchez HA, Veliz LP, Bukauskas FF, Bennett MV, Saez JC (2004) Role of connexin-based gap junction channels and hemichannels in ischemia-induced cell death in nervous tissue. Brain Res Brain Res Rev 47:290–303. doi:10.1016/j.brainresrev.2004.08.002
15. Danik SB, Liu F, Zhang J, Suk HJ, Morley GE, Fishman GI, Gutstein DE (2004) Modulation of cardiac gap junction expression and arrhythmic susceptibility. Circ Res 95:1035–1041. doi:10.1161/01.RES.0000148664.33695.2a
16. De Bock M, Culot M, Wang N, Bol M, Decrock E, De Vuyst E, da Costa A, Dauwe I, Vinken M, Simon AM, Rogiers V, De Ley G, Evans WH, Bultynck G, Dupont G, Cecchelli R, Leybaert L (2011) Connexin channels provide a target to manipulate brain endothelial calcium dynamics and blood-brain barrier permeability. J Cereb Blood Flow Metab 31:1942–1957. doi:10.1038/jcbfm.2011.86
17. De Vuyst E, Decrock E, Cabooter L, Dubyak GR, Naus CC, Evans WH, Leybaert L (2006) Intracellular calcium changes trigger connexin 32 hemichannel opening. EMBO J 25:34–44. doi:10.1038/sj.emboj.7600908
18. De Vuyst E, Decrock E, De Bock M, Yamasaki H, Naus CC, Evans WH, Leybaert L (2007) Connexin hemichannels and gap junction channels are differentially influenced by lipopolysaccharide and basic fibroblast growth factor. Mol Biol Cell 18:34–46. doi:10.1091/mbc.E06-03-0182
19. De Vuyst E, Wang N, Decrock E, De Bock M, Vinken M, Van Moorhem M, Lai C, Culot M, Rogiers V, Cecchelli R, Naus CC, Evans WH, Leybaert L (2009) Ca(2 +) regulation of connexin 43 hemichannels in C6 glioma and glial cells. Cell Calcium 46:176–187. doi:10.1016/j.ceca.2009.07.002
20. de Wit C, Griffith TM (2010) Connexins and gap junctions in the EDHF phenomenon and conducted vasomotor responses. Pflugers Arch 459:897–914. doi:10.1007/s00424-010-0830-4
21. Decrock E, De Vuyst E, Vinken M, Van Moorhem M, Vranckx K, Wang N, Van LL, De Bock M, D'Herde K, Lai CP, Rogiers V, Evans WH, Naus CC, Leybaert L (2009) Connexin 43 hemichannels contribute to the propagation of apoptotic cell death in a rat C6 glioma cell model. Cell Death Differ 16:151–163. doi:10.1038/cdd.2008.138
22. Duffy HS, Sorgen PL, Girvin ME, O'Donnell P, Coombs W, Taffet SM, Delmar M, Spray DC (2002) pH-dependent intramolecular binding and structure involving Cx43 cytoplasmic domains. J Biol Chem 277:36706–36714. doi:10.1074/jbc.M207016200
23. Elenes S, Martinez AD, Delmar M, Beyer EC, Moreno AP (2001) Heterotypic docking of Cx43 and Cx45 connexons blocks fast voltage gating of Cx43. Biophys J 81:1406–1418. doi:10.1016/S0006-3495(01)75796-7
24. Evans WH, Boitano S (2001) Connexin mimetic peptides: specific inhibitors of gap-junctional intercellular communication. Biochem Soc Trans 29:606–612
25. Evans WH, Bultynck G, Leybaert L (2012) Manipulating connexin communication channels: use of peptidomimetics and the translational outputs. J Membr Biol 245:437–449. doi:10.1007/s00232-012-9488-5
26. Evans WH, De VE, Leybaert L (2006) The gap junction cellular internet: connexin hemichannels enter the signalling limelight. Biochem J 397:1–14. doi:10.1042/BJ20060175
27. Harris AL (2001) Emerging issues of connexin channels: biophysics fills the gap. Q Rev Biophys 34:325–472
28. Hawat G, Benderdour M, Rousseau G, Baroudi G (2010) Connexin 43 mimetic peptide Gap26 confers protection to intact heart against myocardial ischemia injury. Pflugers Arch 460:583–592. doi:10.1007/s00424-010-0849-6
29. Hawat G, Helie P, Baroudi G (2012) Single intravenous low-dose injections of connexin 43 mimetic peptides protect ischemic heart in vivo against myocardial infarction. J Mol Cell Cardiol 53:559–566. doi:10.1016/j.yjmcc.2012.07.008
30. Heinzel FR, Luo Y, Li X, Boengler K, Buechert A, Garcia-Dorado D, Di LF, Schulz R, Heusch G (2005) Impairment of diazoxide-induced formation of reactive oxygen species and loss of cardioprotection in connexin 43 deficient mice. Circ Res 97:583–586. doi:10.1161/01.RES.0000181171.65293.65
31. Hirst-Jensen BJ, Sahoo P, Kieken F, Delmar M, Sorgen PL (2007) Characterization of the pH-dependent interaction between

the gap junction protein connexin43 carboxyl terminus and cytoplasmic loop domains. J Biol Chem 282:5801–5813. doi:10.1074/jbc.M605233200
32. Jansen JA, van Veen TA, de Bakker JM, van Rijen HV (2010) Cardiac connexins and impulse propagation. J Mol Cell Cardiol 48:76–82. doi:10.1016/j.yjmcc.2009.08.018
33. Johansen D, Cruciani V, Sundset R, Ytrehus K, Mikalsen SO (2011) Ischemia induces closure of gap junctional channels and opening of hemichannels in heart-derived cells and tissue. Cell Physiol Biochem 28:103–114. doi:10.1159/000331719
34. John SA, Kondo R, Wang SY, Goldhaber JI, Weiss JN (1999) Connexin-43 hemichannels opened by metabolic inhibition. J Biol Chem 274:236–240
35. Kalcheva N, Qu J, Sandeep N, Garcia L, Zhang J, Wang Z, Lampe PD, Suadicani SO, Spray DC, Fishman GI (2007) Gap junction remodeling and cardiac arrhythmogenesis in a murine model of oculodentodigital dysplasia. Proc Natl Acad Sci USA 104:20512–20516. doi:10.1073/pnas.0705472105
36. Kienitz MC, Bender K, Dermietzel R, Pott L, Zoidl G (2011) Pannexin 1 constitutes the large conductance cation channel of cardiac myocytes. J Biol Chem 286:290–298. doi:10.1074/jbc.M110.163477
37. Kim DY, Kam Y, Koo SK, Joe CO (1999) Gating connexin 43 channels reconstituted in lipid vesicles by mitogen-activated protein kinase phosphorylation. J Biol Chem 274:5581–5587
38. Kondo RP, Wang SY, John SA, Weiss JN, Goldhaber JI (2000) Metabolic inhibition activates a non-selective current through connexin hemichannels in isolated ventricular myocytes. J Mol Cell Cardiol 32:1859–1872. doi:10.1006/jmcc.2000.1220
39. Lai A, Le DN, Paznekas WA, Gifford WD, Jabs EW, Charles AC (2006) Oculodentodigital dysplasia connexin43 mutations result in non-functional connexin hemichannels and gap junctions in C6 glioma cells. J Cell Sci 119:532–541. doi:10.1242/jcs.02770
40. Li X, Heinzel FR, Boengler K, Schulz R, Heusch G (2004) Role of connexin 43 in ischemic preconditioning does not involve intercellular communication through gap junctions. J Mol Cell Cardiol 36:161–163
41. Locke D, Liu J, Harris AL (2005) Lipid rafts prepared by different methods contain different connexin channels, but gap junctions are not lipid rafts. Biochemistry 44:13027–13042. doi:10.1021/bi050495a
42. Locovei S, Bao L, Dahl G (2006) Pannexin 1 in erythrocytes: function without a gap. Proc Natl Acad Sci USA 103:7655–7659. doi:10.1073/pnas.0601037103
43. Maass K, Shibayama J, Chase SE, Willecke K, Delmar M (2007) C-terminal truncation of connexin43 changes number, size, and localization of cardiac gap junction plaques. Circ Res 101:1283–1291. doi:10.1161/CIRCRESAHA.107.162818
44. Miro-Casas E, Ruiz-Meana M, Agullo E, Stahlhofen S, Rodriguez-Sinovas A, Cabestrero A, Jorge I, Torre I, Vazquez J, Boengler K, Schulz R, Heusch G, Garcia-Dorado D (2009) Connexin43 in cardiomyocyte mitochondria contributes to mitochondrial potassium uptake. Cardiovasc Res 83:747–756. doi:10.1093/cvr/cvp157
45. Miura T, Miki T, Yano T (2010) Role of the gap junction in ischemic preconditioning in the heart. Am J Physiol Heart Circ Physiol 298:H1115–H1125. doi:10.1152/ajpheart.00879.2009
46. Miura T, Ohnuma Y, Kuno A, Tanno M, Ichikawa Y, Nakamura Y, Yano T, Miki T, Sakamoto J, Shimamoto K (2004) Protective role of gap junctions in preconditioning against myocardial infarction. Am J Physiol Heart Circ Physiol 286:H214–H221. doi:10.1152/ajpheart.00441.2003
47. Oviedo-Orta E, Errington RJ, Evans WH (2002) Gap junction intercellular communication during lymphocyte transendothelial migration. Cell Biol Int 26:253–263. doi:10.1006/cbir.2001.0840
48. Pelegrin P, Surprenant A (2006) Pannexin-1 mediates large pore formation and interleukin-1beta release by the ATP-gated P2X7 receptor. EMBO J 25:5071–5082. doi:10.1038/sj.emboj.7601378
49. Ponsaerts R, De Vuyst E, Retamal M, D'hondt C, Vermeire D, Wang N, De Smedt H, Zimmermann P, Himpens B, Vereecke J, Leybaert L, Bultynck G (2010) Intramolecular loop/tail interactions are essential for connexin 43-hemichannel activity. FASEB J 24:4378–4395. doi:10.1096/fj.09-153007
50. Ponsaerts R, Wang N, Himpens B, Leybaert L, Bultynck G (2012) The contractile system as a negative regulator of the connexin 43 hemichannel. Biol Cell 104:367–377. doi:10.1111/boc.201100079
51. Ramachandran S, Xie LH, John SA, Subramaniam S, Lal R (2007) A novel role for connexin hemichannel in oxidative stress and smoking-induced cell injury. PLoS One 2:e712. doi:10.1371/journal.pone.0000712
52. Retamal MA, Cortes CJ, Reuss L, Bennett MV, Saez JC (2006) S-nitrosylation and permeation through connexin 43 hemichannels in astrocytes: induction by oxidant stress and reversal by reducing agents. Proc Natl Acad Sci USA 103:4475–4480. doi:10.1073/pnas.0511118103
53. Retamal MA, Schalper KA, Shoji KF, Bennett MV, Saez JC (2007) Opening of connexin 43 hemichannels is increased by lowering intracellular redox potential. Proc Natl Acad Sci USA 104:8322–8327. doi:10.1073/pnas.0702456104
54. Retamal MA, Schalper KA, Shoji KF, Orellana JA, Bennett MV, Saez JC (2007) Possible involvement of different connexin43 domains in plasma membrane permeabilization induced by ischemia-reperfusion. J Membr Biol 218:49–63. doi:10.1007/s00232-007-9043-y
55. Rhett JM, Jourdan J, Gourdie RG (2011) Connexin 43 connexon to gap junction transition is regulated by zonula occludens-1. Mol Biol Cell 22:1516–1528. doi:10.1091/mbc.E10-06-0548
56. Rodriguez-Sinovas A, Boengler K, Cabestrero A, Gres P, Morente M, Ruiz-Meana M, Konietzka I, Miro E, Totzeck A, Heusch G, Schulz R, Garcia-Dorado D (2006) Translocation of connexin 43 to the inner mitochondrial membrane of cardiomyocytes through the heat shock protein 90-dependent TOM pathway and its importance for cardioprotection. Circ Res 99:93–101. doi:10.1161/01.RES.0000230315.56904.de
57. Rodriguez-Sinovas A, Sanchez JA, Fernandez-Sanz C, Ruiz-Meana M, Garcia-Dorado D (2012) Connexin and pannexin as modulators of myocardial injury. Biochim Biophys Acta 1818:1962–1970. doi:10.1016/j.bbamem.2011.07.041
58. Saez JC, Schalper KA, Retamal MA, Orellana JA, Shoji KF, Bennett MV (2010) Cell membrane permeabilization via connexin hemichannels in living and dying cells. Exp Cell Res 316:2377–2389. doi:10.1016/j.yexcr.2010.05.026
59. Sanchez HA, Orellana JA, Verselis VK, Saez JC (2009) Metabolic inhibition increases activity of connexin-32 hemichannels permeable to $Ca^{2+}$ in transfected HeLa cells. Am J Physiol Cell Physiol 297:C665–C678. doi:10.1152/ajpcell.00200.2009
60. Sanchez JA, Rodriguez-Sinovas A, Fernandez-Sanz C, Ruiz-Meana M, Garcia-Dorado D (2011) Effects of a reduction in the number of gap junction channels or in their conductance on ischemia-reperfusion arrhythmias in isolated mouse hearts. Am J Physiol Heart Circ Physiol 301:H2442–H2453. doi:10.1152/ajpheart.00540.2011
61. Schulz R, Boengler K, Totzeck A, Luo Y, Garcia-Dorado D, Heusch G (2007) Connexin 43 in ischemic pre- and postconditioning. Heart Fail Rev 12:261–266. doi:10.1007/s10741-007-9032-3
62. Schwanke U, Konietzka I, Duschin A, Li X, Schulz R, Heusch G (2002) No ischemic preconditioning in heterozygous connexin43-deficient mice. Am J Physiol Heart Circ Physiol 283:H1740–H1742. doi:10.1152/ajpheart.00442.2002
63. Seki A, Coombs W, Taffet SM, Delmar M (2004) Loss of electrical communication, but not plaque formation, after mutations in the cytoplasmic loop of connexin43. Heart Rhythm 1:227–233. doi:10.1016/j.hrthm.2004.03.066

64. Severs NJ, Bruce AF, Dupont E, Rothery S (2008) Remodelling of gap junctions and connexin expression in diseased myocardium. Cardiovasc Res 80:9–19. doi:10.1093/cvr/cvn133
65. Shibayama J, Paznekas W, Seki A, Taffet S, Jabs EW, Delmar M, Musa H (2005) Functional characterization of connexin43 mutations found in patients with oculodentodigital dysplasia. Circ Res 96:e83–e91. doi:10.1161/01.RES.0000168369.79972.d2
66. Shintani-Ishida K, Uemura K, Yoshida K (2007) Hemichannels in cardiomyocytes open transiently during ischemia and contribute to reperfusion injury following brief ischemia. Am J Physiol Heart Circ Physiol 293:H1714–H1720. doi:10.1152/ajpheart.00022.2007
67. Silverman WR, de Rivero Vaccari JP, Locovei S, Qiu F, Carlsson SK, Scemes E, Keane RW, Dahl G (2009) The pannexin 1 channel activates the inflammasome in neurons and astrocytes. J Biol Chem 284:18143–18151. doi:10.1074/jbc.M109.004804
68. Spray DC, Ye ZC, Ransom BR (2006) Functional connexin "hemichannels": a critical appraisal. Glia 54:758–773. doi:10.1002/glia.20429
69. Stankovicova T, Szilard M, De S,I, Sipido KR (2000) M cells and transmural heterogeneity of action potential configuration in myocytes from the left ventricular wall of the pig heart. Cardiovasc Res 45:952–960
70. Thompson RJ, Jackson MF, Olah ME, Rungta RL, Hines DJ, Beazely MA, MacDonald JF, MacVicar BA (2008) Activation of pannexin-1 hemichannels augments aberrant bursting in the hippocampus. Science 322:1555–1559. doi:10.1126/science.1165209
71. Tribulova N, Seki S, Radosinska J, Kaplan P, Babusikova E, Knezl V, Mochizuki S (2009) Myocardial $Ca^{2+}$ handling and cell-to-cell coupling, key factors in prevention of sudden cardiac death. Can J Physiol Pharmacol 87:1120–1129. doi:10.1139/Y09-106
72. Unwin PN, Ennis PD (1983) Calcium-mediated changes in gap junction structure: evidence from the low angle X-ray pattern. J Cell Biol 97:1459–1466
73. Unwin PN, Zampighi G (1980) Structure of the junction between communicating cells. Nature 283:545–549
74. Veenstra RD, DeHaan RL (1986) Measurement of single channel currents from cardiac gap junctions. Science 233:972–974
75. Vergara L, Bao X, Bello-Reuss E, Reuss L (2003) Do connexin 43 gap-junctional hemichannels activate and cause cell damage during ATP depletion of renal-tubule cells? Acta Physiol Scand 179:33–38
76. Wang J, Ma M, Locovei S, Keane RW, Dahl G (2007) Modulation of membrane channel currents by gap junction protein mimetic peptides: size matters. Am J Physiol Cell Physiol 293:C1112–C1119. doi:10.1152/ajpcell.00097.2007
77. Wang N, De Bock M, Antoons G, Gadicherla AK, Bol M, Decrock E, Evans WH, Sipido KR, Bukauskas FF, Leybaert L (2012) Connexin mimetic peptides inhibit Cx43 hemichannel opening triggered by voltage and intracellular $Ca^{2+}$ elevation. Basic Res Cardiol 107:304. doi:10.1007/s00395-012-0304-2
78. Warner A, Clements DK, Parikh S, Evans WH, DeHaan RL (1995) Specific motifs in the external loops of connexin proteins can determine gap junction formation between chick heart myocytes. J Physiol 488(Pt 3):721–728
79. Wright CS, van Steensel MA, Hodgins MB, Martin PE (2009) Connexin mimetic peptides improve cell migration rates of human epidermal keratinocytes and dermal fibroblasts in vitro. Wound Repair Regen 17:240–249. doi:10.1111/j.1524-475X.2009.00471.x
80. Yang XM, Liu Y, Liu Y, Tandon N, Kambayashi J, Downey JM, Cohen MV (2010) Attenuation of infarction in cynomolgus monkeys: preconditioning and postconditioning. Basic Res Cardiol 105:119–128. doi:10.1007/s00395-009-0050-2